Supplement to: Submesoscale effects on changes to export production under global warming

Genevieve Jay Brett[1,2], Daniel B Whitt[3,4], Matthew C Long[4], Frank O. Bryan[4], Kate Feloy[2], Kelvin J. Richards[2]

[1]Johns Hopkins University Applied Physics Laboratory 11100 Johns Hopkins Road, Laurel, MD 20723, USA

[2]University of Hawai'i Manoa 1680 East West Road, Honolulu HI 96822, USA

[3]Ames Research Center, National Aeronautics and Space Administration, Moffett Field, CA, USA

[4]Climate and Global Dynamics Laboratory, National Center for Atmospheric Research, Boulder, CO, USA

S1 Physical Model

In this section we provide more detail on the physical model setup and the seasonal cycle of mixed layer depth, temperature, salinity, and squared vertical velocities. For further discussion of the physics, see Richards et al. (2021), which uses nearly-identical simulations.

We use the Regional Ocean Modeling System (ROMS) with a 4km grid to model the Porcupine Abyssal Plain region in the North Atlantic, specifically 41-51°N and 11-27°W. This regional model is in a one-way-nested configuration within a Community Earth System Model (CESM) version 2.0 global model in an "ocean-sea-ice" configuration at a nominal 0.1°forced by atmospheric fields derived from reanalysis representative of a statistically normal annual cycle, i.e. a normal year (Large & Yeager, 2004). To develop a process-oriented means of examining the response of new production and vertical export fluxes to idealized changes in climate, we utilize the "time slice" approach for our global model, as described in Richards et al. (2021) and Brett et al. (2021). Thus, the global model's initial conditions and both models' surface forcing are set to simulate a period representative of either early- or late-century climate conditions, with the adjust-

Corresponding author: Jay Brett, Jay.Brett@jhuapl.edu

ments for late-century conditions set by anomalies computed from the fully-coupled CESM1 Large Ensemble (CESM-LE; Kay et al., 2015).

Richards et al. (2021) provide details of the ROMS setup for a 1.25km and 4km resolution grid nested within the same global model runs. The regional model is initialized with February first conditions and run for 4 years. Here we use only the 4km grid with 90 vertical levels, as we saw very small differences between 1.25km and 4km output. To suppress a portion of the submesoscale in what we call the *viscous* runs, as opposed to *standard* runs, we increase the viscosity and diffusivity via increasing the hyperdiffusivity and hyperviscosity coefficients by a factor of 64, which damps but does not eliminate wavelengths below 60km. The comparison between the two cases will allow us to explicitly quantify the impact of the resolved submesoscales in the standard run. Each simulation is run for 3.5 years.

In the 2000s climate, the mixed layer shows a seasonal cycle with its maximum in March near 215m depth, followed by spring shallowing that is interrupted by a noticeable but short storm-induced remixing at the end of April. This cycle is shown in figureS1 as the mean over the domain and three model years, from 6 months after initialization onward. The mixed layer is shallow throughout the summer, with fall mixing noticeable starting in October. The main point of difference between the standard and viscous runs is associated with the April storm, which remixes the viscous run deeper than the standard, with the mixed layer depth reaching 100m rather than 60m.

The increased viscosity has very little impact on area-mean temperature, salinity, and potential density fields throughout the year (figure S1), with temperature differences within 0.5°C, salinity differences within 0.1psu, and densities within 0.05kg/m^3. However, the viscous run has slightly cooler, fresher, denser water just below the mixed layer depth in the summer and fall, with slightly cooler, fresher, less dense water within the mixed layer in the fall to winter. The different signs of the density differences are due to asymmetries between temperature and salinity differences during the two time periods. The mean squared vertical components of velocity show the largest effects of increased viscosity, with winter maximum values being about 60% lower in the viscous run. As these velocities are directly impacted by viscosity, this is to be expected.

In the warmer climate, the mixed layer depth has a shallower March maximum near 75m (figureS2 shows the domain and 3-year mean seasonal cycle, from 6 months after

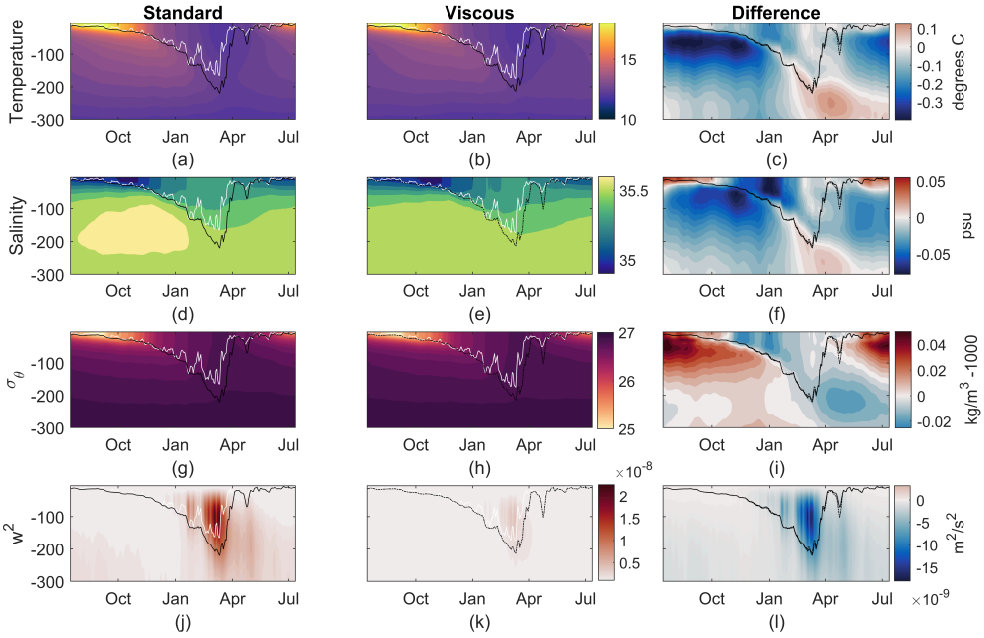

Figure S1: Domain and 3-year mean of temperature (a,b), salinity (d,e), potential density (g,h), and squared vertical component of velocity (j,k) for the 2000s climate. Left column is the standard run (a,d,g,j), middle the high-viscosity run (b,e,h,k), and right the difference, viscous-standard (c,f,i,l). White curves are the boundary layer depth, black curves the mixed layer depth. In the rightmost column, the standard run's mixed layer depth curve is solid while the viscous run's is dashed.

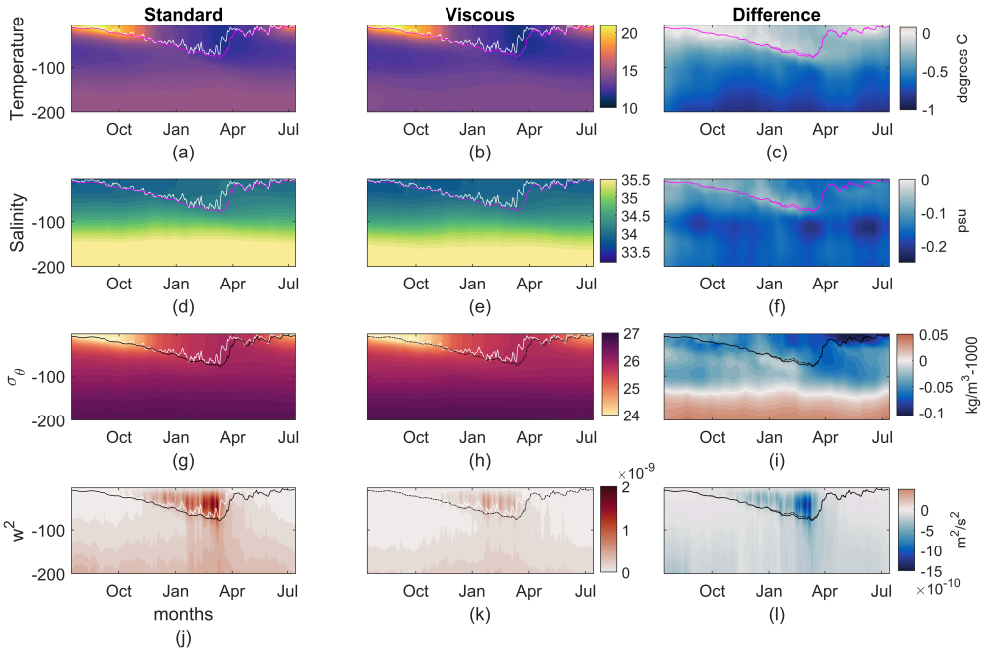

Figure S2: Domain and 3-year mean of temperature (a,b), salinity (d,e), potential density (g,h), and squared vertical component of velocity (j,k) for the 2100s climate. Left column is the standard run (a,d,g,j), middle the high-viscosity run (b,e,h,k), and right the difference, viscous-standard (c,f,i,l). White curves are the boundary layer depth, black and magenta curves the mixed layer depth. In the rightmost column, the standard run's mixed layer depth curve is solid while the viscous run's is dashed.

initialization onward). There is no qualitative difference between the standard and viscous mixed layer depths, and the April storm's effects are much less noticeable. The surface water is warmer, fresher, and less dense than in the 2000s climate, as imposed by the initial and boundary conditions. The viscous runs are cooler, fresher, and less dense than the standard runs throughout the top 150m, which includes the deepest mixed layer depths. As in the 2000s climate, these differences are small. In contrast, the differences in mean squared vertical components of velocity is again large. The standard run in 2100s has maximum w^2 about 10% of those in the 2000s standard run. The viscous run in 2100s has maximum w^2 about 40% of those in the standard run, the same ratio as in the 2000s runs.

To demonstrate the specific variability reduced in the viscous run compared to the standard run, we show spectra of horizontal and vertical kinetic energy. These spectra focus on the winter mixed layer, when there is the most submesoscale activity. In the 2000s, spectra are at 100m, within the winter mixed layer, and in the 2100s, spectra are at 50m to remain within that winter mixed layer. Spectra are from the snapshots every 5 days. The horizontal kinetic energy spectra, figure S3, do not have a strong seasonal cycle. Maximum horizontal kinetic energy is at wavelengths near 150-210km in all runs. The viscous run has largely reduced kinetic energy below about 60km (-4.8 on the plot y-axes, the log of cycles per meter). Vertical kinetic energy spectra have a strong seasonal cycle, as shown for the vertical velocity in the main text, and so are averaged over the years of the run to show the average seasonal cycle, figure S4. The maximum vertical kinetic energy in the winter is near 19km wavelengths in the standard run and 33km in the viscous run in the 2000s, and 22km in the standard run and 39km in the viscous run in the 2100s. That is to say the vertical kinetic energy is largest near wavelength of 5 grid points in the standard run and 9 grid points in the viscous run. The ratio between the most energetic winter wavelengths is approximately 1.75 (viscous:standard), and there is also a reduction of the maximum energy at those wavelengths by about a factor of 2.

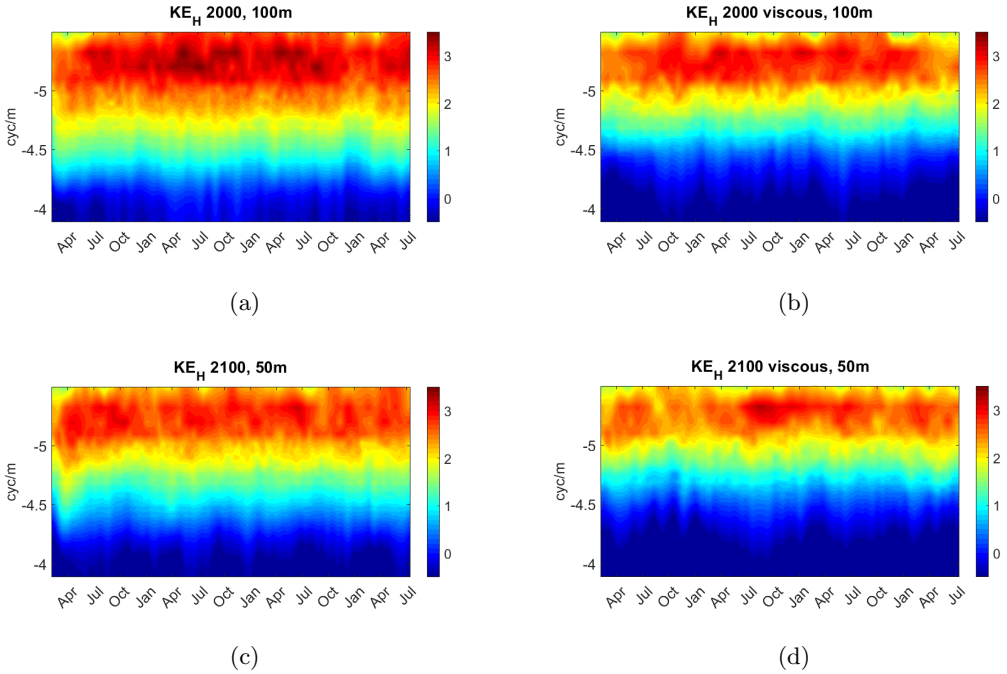

Figure S3: Spectra of the horizontal kinetic energy. Colors are the log (base 10) of the energy, and the y-axes are the log (base 10) of the wavelengths in cycles per meter. (a,b) 2000s, 100m depth. (c,d) 2100s, 50m depth. (a,c) standard runs. (b,d) viscous runs.

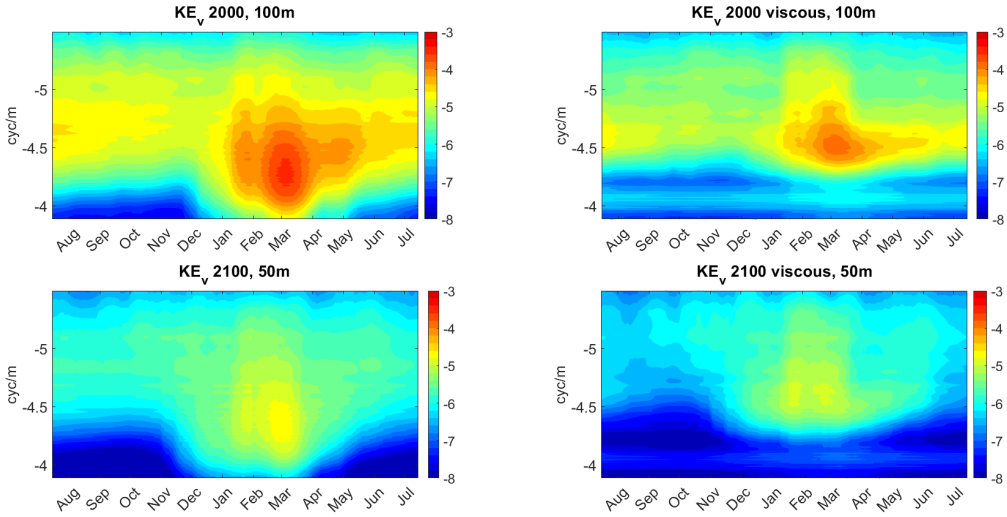

Figure S4: Spectra of the vertical kinetic energy, averaged over the model run years to show the average seasonal cycle. Colors are the log (base 10) of the energy, and the y-axes are the log (base 10) of the wavelengths in cycles per meter. (a,b) 2000s, 100m depth. (c,d) 2100s, 50m depth. (a,c) standard runs. (b,d) viscous runs.

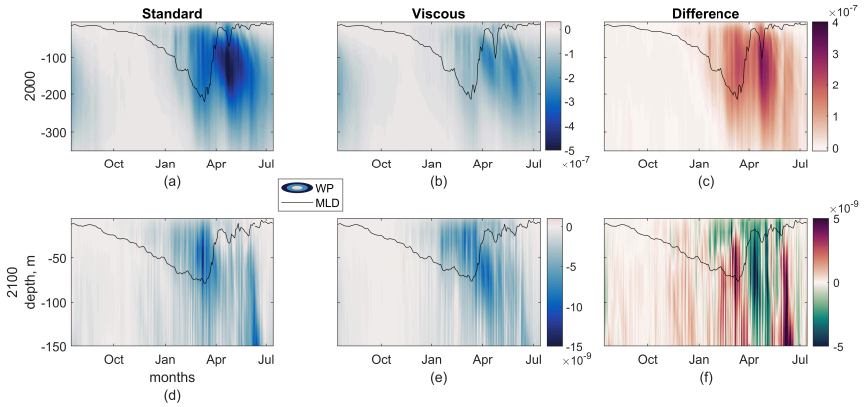

Figure S5: Submesoscale vertical advective particle fluxes from 36hr-mean w and P with spatial mean and linear trends removed. Compare with figure 9 in the main text.

S2 Submesoscale Analysis

Submesoscale fluxes in the main text are found by removing a mesoscale component from both the vertical component of the velocity and the relevant concentration (buoyancy, nutrient, particle) to reach a submesoscale component for both and using the product of those components. Here we show that the results qualitatively match an alternate method, removing just the mean and a linear trend across the domain from each component. Submesoscale particle fluxes are shown in figure S5 (compare to figure 11) and submesoscale buoyancy fluxes are shown in figure S6 (compare to figure 12).

S3 Alternate Boundary Condition Flux Results

While in the main text we have focused on the results using the constant WOA-based nutrient-density relationship at the boundaries, here we include results on the export flux with the altered 2100s boundary condition, constructed using the CESM-LE nutrient-density relationship anomalies. Recall that figure 5 in the main text shows the production rate, and that the magnitudes of the vertical component of velocity will be the same as discussed in the main text.

The early-century cases shown here are the same as in figure 8 of the main text. In the late-century cases, the total flux is 3.6% larger in the viscous than the standard case, mainly due to a 3.5% larger gravitational component. These differences in the total and gravitational fluxes between standard and viscous runs are small compared to

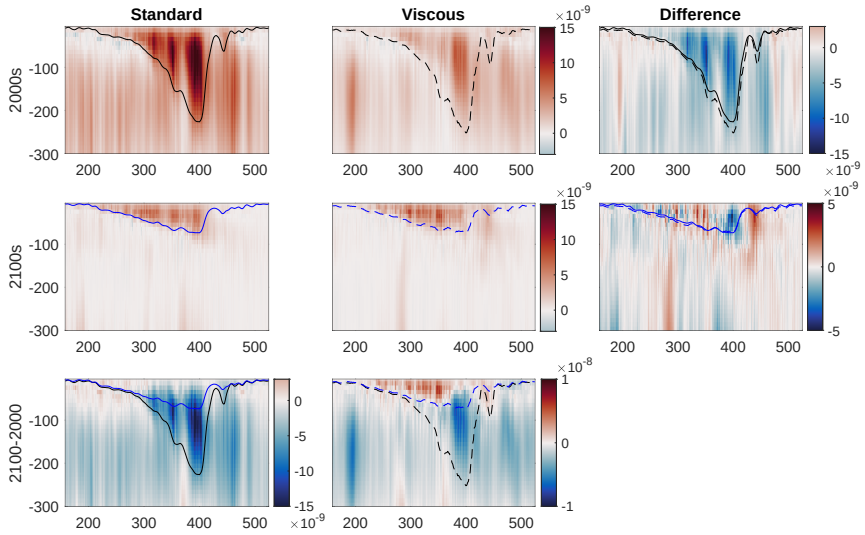

Figure S6: Vertical buoyancy fluxes from 36hr-mean w and b with spatial mean and linear trends removed. Compare with figure 10 in the main text.

the reduction in the total flux with a warmer climate of 37% for the standard cases and 32% for the viscous cases.

Results are consistent regardless of boundary conditions, with particle advective fluxes showing larger effects of both viscosity and climate than the gravitational fluxes. In the 2100s, the advective fluxes are much smaller than in the 2000s, reduced by 64.7% for the standard and 31.3% for the viscous case, and more similar, with the viscous case 5.1% larger. The submesoscale components show yet larger effects: $w'P'$ is 53.6% larger in the standard case in the warmer climate. The reductions with warming are 86% for the standard case, larger than the 64.0% in the viscous case.

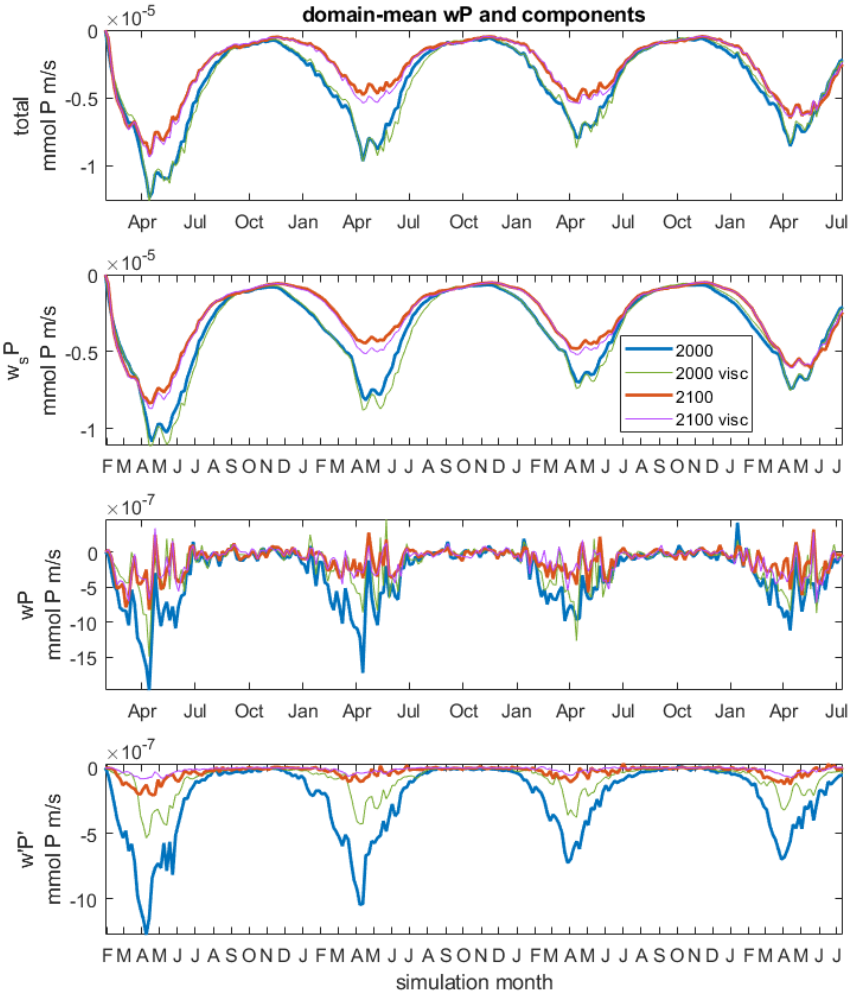

Figure S7: Vertical flux of plankton at 100m depth; mmol m/s. Top, total. 2nd row, only gravitational sinking component. 3rd row, only advective component. Bottom, sub-mesoscale portion of advective component. In all rows, colors indicate which of 4 runs is represented, differentiating standard and viscous runs in both 2000s and 2100s climate. All simulations use $w_s = 5md^{-1}$ and $\tau = 50$days. Compare with figure 8 in the main text.

References

Brett, G. J., Whitt, D. B., Long, M. C., Bryan, F., Feloy, K., & Richards, K. J. (2021). Sensitivity of 21st-century projected ocean new production changes to idealized biogeochemical model structure. *Biogeosciences Discussions*, 1–32.

Kay, J., Deser, C., Phillips, A., Mai, A., Hannay, C., Strand, G., ... others (2015). The community earth system model (cesm) large ensemble project: A community resource for studying climate change in the presence of internal climate variability. *Bulletin of the American Meteorological Society*, *96*(8), 1333–1349.

Large, W. G., & Yeager, S. G. (2004). *Diurnal to decadal global forcing for ocean and sea-ice models: The data sets and flux climatologies* (Vols. TechnicalReport TN-460+STR).

Richards, K. J., Whitt, D. B., Brett, G. J., Bryan, F. O., Feloy, K., & Long, M. C. (2021). The impact of climate change on ocean submesoscale activity. *Journal of Geophysical Research: Oceans*, *126*(5), e2020JC016750.